Control of Cell Growth Direction by Direct Fabrication of Periodic Micro- and Submicrometer Arrays on Polymers

Denise Langheinrich,[1] Edith Yslas,[2] Martín Broglia,[2] Viviana Rivarola,[2] Diego Acevedo,[2] Andrés Lasagni[1]

[1]Fraunhofer Institute for Material and Beam Technology, Winterbergstraße 28, 01277 Dresden, Germany

[2]Universidad Nacional de Rio Cuarto, Departamento de Química, Ruta 36 Km 601, Río Cuarto, Córdoba 5800, Argentina

Correspondence to: A. Lasagni (E-mail: andres-fabian.lasagni@iws.fraunhofer.de)

Received 8 August 2011; accepted 15 November 2011; published online 15 December 2011
DOI: 10.1002/polb.23017

ABSTRACT: In this work, we describe a laser-assisted microstructuring technique called Direct Laser Interference Patterning to produce topographical cues for tumor cells in a one-step process. Line-like patterns with spatial periods ranging from 500 nm to 10 μm are fabricated on polyimide (PI) films. The resulting structures exhibit a well-defined shape and quality even for patterns with small periodic distances. Subsequently, the behavior of mouse mammary adenocarcinoma cells over those structures is evaluated. The results show that cell growth is well aligned to the direction of the patterns (over 60% lying within 0° to 15° to either side of the surface lines) for all evaluated structure sizes. Moreover, cells grown on patterns with 500 nm spatial period are the most narrowly aligned (up to 80% found between 0° and 15°), showing the potential of the technique. The fabrication process of the PI patterns is supported by a mathematical model of the underlying photo-chemical ablation process. © 2011 Wiley Periodicals, Inc. J Polym Sci Part B: Polym Phys 50: 415–422, 2012

KEYWORDS: biomaterials; cell guidance; Direct Laser Interference Patterning; laser ablation; polyimide; surfaces

INTRODUCTION Micro- and nano-structured surfaces have gained increasing prominence in medicine, cell biology, and other biological fields of research in the past few years.[1–5] In particular, it has been found that patterning on solid substrates can be used not only to control cell adhesion and growth but also to regulate cell functions. In this regard, novel application fields such as biomolecular and cell analysis, microfluidics, biomedical drug delivery, and medical prostheses are developing at a rapid pace. However, the further development of these technologies greatly depends on being able to produce substrates in an easy, fast, and economical way, while simultaneously improving our understanding of the cell-substratum interactions.[2]

According to the most recent studies, cells can actively adapt to the surface on which they adhere, activating specific intracellular signals that can influence cell survival and behavior.[6–8]

To incorporate biological cues on the surface of polymers, a useful strategy is to modify their macromolecules chemically and/or physically. Chemical modification has been extensively investigated by anchoring biomolecules[9–11] or by immobilizing bioactive moieties onto the surface of the material.[12–14] Physical modification has been performed using various methods to alter surface roughness or otherwise change the topography to display a desired characteristic.[15,16] In the last case, several reports have shown that the depth and pitch of grooves will determine the cellular response to the patterned surfaces. However, there is no common adhesion trend across various cells and cell lines,[17,18] while the scale of the microtopography needs to be optimized for different types of cell adhesion.[19,20] The range of topographic scale that induces contact guidance has not yet been fully determined but strongly depends on the cell type and substrate material.[2,21] In the past, several techniques have been used to produce repetitive surface patterning. These methods normally require multiple steps to fabricate the final micro- and submicrometer ordered surface. In optical lithography, for example, a photoresist is exposed to a light source through a photo mask featuring the shape of the pattern to be reproduced, after which the sample must be developed and etched to obtain the final structure.[22] Other methods such as electron or ion beam lithography, as well as laser writing, have been used to directly print different patterns on the polymers by scanning the beam on the surface.[8,23] However, long processing times (e.g., for electron and ion beam lithography) are necessary, especially if large areas (several cm^2) are to be processed.[9,23,24]

A promising technology which permits direct fabrication of periodic arrays on different kinds of solid materials such as polymers, metals, and ceramics is Direct Laser Interference

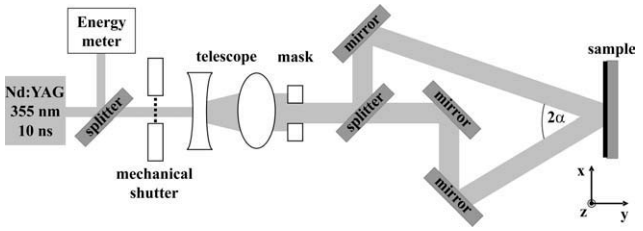

FIGURE 1 Experimental setup for the patterning of PI surfaces with the DLIP method (two beam configuration).

Patterning (DLIP). DLIP uses the interference of two or more laser beams to offer rapid fabrication with a high degree of design flexibility.[12,25,26] This is only possible when an accurate spatial and temporal overlap of the laser pulses from all interfering laser beams is ensured. Because high energetic laser pulses are used, the materials can be processed in one step, thereby obviating the use of a photoresist with the subsequent stages of developing and etching the substrate. Furthermore, it is possible to generate structures in several square millimeters using just a single laser pulse.

In this study, DLIP has been used to fabricate line-like arrays on polyimide (PI) substrates, which serve as templates for cell growth experiments with mouse mammary adenocarcinoma cells (LM2). Although this method has been previously used to investigate contact cell guidance investigations of fibroblast on polycarbonate coated with collagen,[27] no systematic quantification of cell growth orientation as a function of structure period of the patterns fabricated using DLIP has previously been performed. In addition, this study investigates the shape of the topological features that can be directly obtained on PI substrates as a function of the spatial period (from 500 nm to 10 μm) using a single laser pulse. Furthermore, a mathematical model to describe the mechanism of the structuring process is presented, which together with the experimental observations should determine the limits of DLIP for the processing of PI. The samples are characterized using scanning electron microscopy (SEM), atomic force microscopy (AFM), laser scanning microscopy (LSM), as well as fluorescence microscopy for observation of the cells.

EXPERIMENTAL

Patterning of PI Film

PI films purchased from Goodfellow GmbH (Bad Nauheim, Germany) with a thickness of 125 μm were used for the experiments. To fabricate the periodic structures, a high-power pulsed (pulse duration: 10 ns, repetition rate: 10 Hz), frequency tripled Nd:YAG laser (Quanta Ray, Spectra Physics) was used to produce a linearly polarized beam of wavelength 355 nm. The experimental setup for the two laser beam configuration is shown in Figure 1. After passing through the telescope and mask, the primary laser beam was divided into two coherent beams using a 50% reflective beam splitter. The mirrors were positioned to ensure that the laser beams interfered on the sample surface. The spatial period was varied between 500 nm and 10 μm by adjusting the intercepting angle between the beams (2α). All experiments were performed at ambient conditions of pressure and temperature.

Sample Characterization

A SEM (XL30 ESEM-SEG, Philips) with an operating voltage of 5 kV was used to visualize the patterned PI surfaces. The structure width and depth of the periodic arrays were measured by LSM (LM5 Pascal, Carl Zeiss MicroImaging GmbH) and AFM. The AFM measurements were made with the Nanowizard 2® (JPK Instruments) using the contact mode.

Cell Culture and Characterization

A mouse mammary adenocarcinoma cell line (LM2) was obtained from Roffo Hospital (Buenos Aires, Argentina) and maintained in Dulbecco's modified Eagle's medium supplemented with 10% fetal bovine serum, 1% L-glutamine, and 1% antibiotic/antimycotic solution at 37 °C in a humid atmosphere of 5% CO_2.

Before cell culture, the PI substrates were rinsed with bidistillated water in an ultrasonic bath for 5 min to remove ablation products produced by the laser treatment and sterilized with ultraviolet radiation for 30 min. After that, LM2 cells (2×10^5) were plated onto the PI samples in 2 mL medium and incubated at 37 °C in a moisturized atmosphere with 5% CO_2. The culture was left for 96 h. The medium was refreshed during the course of this study. The cells were fixed onto the sample surface using cold methanol (−20 °C).

The cell nuclei were then stained with Hoechst 33258 solution (0.5 mg mL^{-1}, Sigma Aldrich, Germany) for 1 min and then washed with water. Afterward, the cells were visualized using a fluorescence and optical microscope (Axiophot, Carl Zeiss Jena, Germany) with a color digital camera (Axiocam, Carl Zeiss Jena, Germany) and the Axiovision 4.3 software. The appropriate filters were used for fluorescence imaging (330–380 nm excitations and emission at 420–450 nm). As reference, LM2 cells were also grown on nonpatterned PI surfaces.

To characterize the cell behavior on the patterned PI surface, the alignment of cells with respect to the lines of the micro- and submicrometer patterns was measured. The degree of alignment was quantified as the angle formed between the axis of the line-like features and the cells. The angle of orientation reflects how closely the cells were aligned with the direction of the lines. The results are classified into six groups: The first group (0°–15°) designates cells, which are either parallel to the line-like features (0°) or fall within 15° (either to the right or left) of line direction; the second group designates those cells with an orientation of 15°–30° (either right or left) from the pattern direction, and so forth. On the nonpatterned PI surface, the lower edge of the sample was defined as the reference line.

RESULTS

DLIP of PI Films

Line-like periodic arrays were produced on the PI substrates using a two beam laser interference setup (Fig. 1). The spatial period (Λ) was varied from 500 nm to 10 μm by adjusting the experimental setup, as this period depends only on

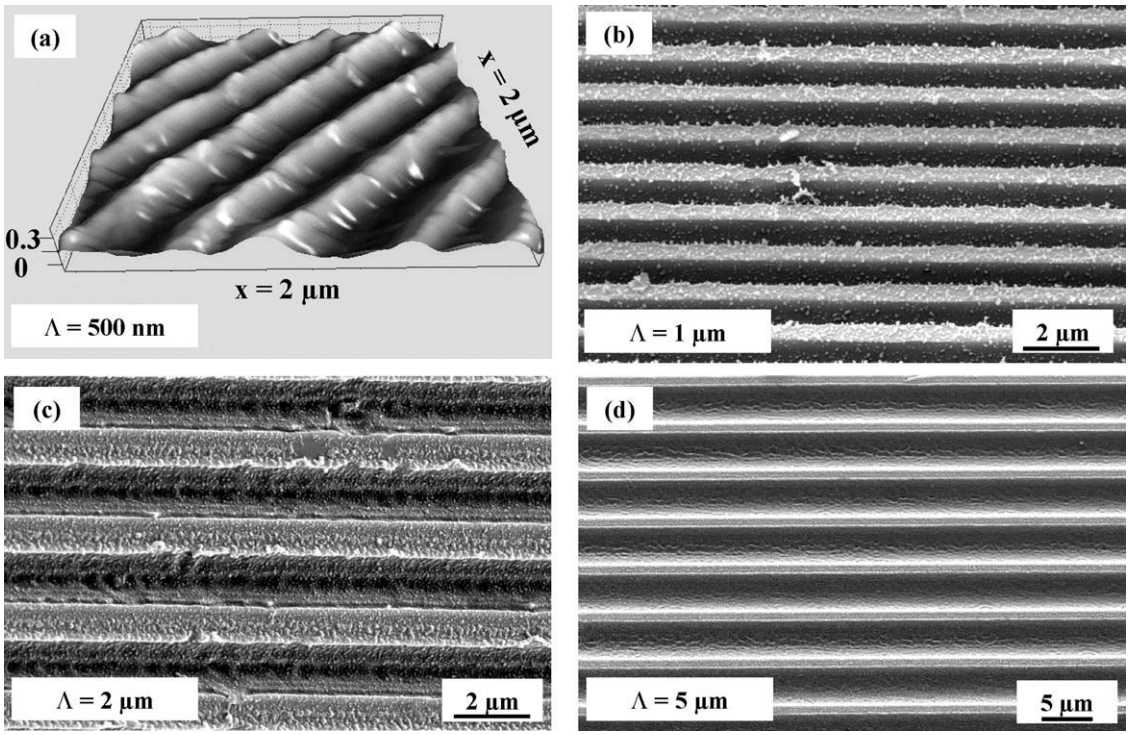

FIGURE 2 AFM (a) and SEM (b–d) images of the line-like patterns on PI surfaces with a spatial period of (a) 500 nm ($F = 0.3$ J cm^{-2}), (b) 1 μm ($F = 0.5$ J cm^{-2}, before rinsing), (c) 2 μm ($F = 0.7$ J cm^{-2}, after rinsing), and (d) 5 μm ($F = 1.0$ J/cm^{-2}, after rinsing).

the laser wavelength ($\lambda = 355$ nm) and the angle between the laser beams (2α) (eq 1):

$$\Lambda = \frac{\lambda}{2 \sin \alpha} \tag{1}$$

The laser fluence (F) was selected with regard to the optimal structure quality (e.g., avoiding collapse of the fabricated array) for each spatial period. For our experiments, the range of laser fluence was 0.2 to 1.0 J cm^{-2}. It was observed that for small spatial periods, laser fluences $\sim$ 0.3, 0.4, and 0.7 J cm^{-2} preserved the morphology of the patterns for 0.5, 1.0, and 2.0 μm arrays, respectively.

Typical examples of the PI surface patterning with a line-like structure are presented in Figure 2(a–d). As can be seen on the SEM images in Figure 2(b–d), the fabricated lines show a distinct shape with precise edges, especially for spatial periods 1, 2, and 5 μm. For the PI substrate with a spatial period of 500 nm shown in the 3D-AFM image of Figure 2(a), the ridges of the lines are rounded with no sharp edging. Furthermore, Figure 2(b) reveals debris ($\sim$ 50–100 nm), which was redeposited on the surface of the sample during laser treatment. The small particles are attached more or less loosely to the samples and can be removed by rinsing the substrate with isopropanol or DI water in an ultrasonic bath [Fig. 2(c,d)].

The surface profiles (dark lines) depicted in Figure 3(a–d), measured using LSM and AFM, show the morphological shape of the surface for each spatial period. To analyze the structure, both the ridge width and the structure depth were measured. The ridge width varied between 117 nm ($\Lambda =$ 500 nm) and 1.55 μm ($\Lambda = 5$ μm). In addition, Figure 3(e) describes the relationship between the spatial period and maximal structure depth, as well as the maximal obtainable aspect ratio (up to a laser energy density of 1.0 J cm^{-2} and one laser pulse). The aspect ratio is defined as the ratio between the structure depth (d) and the spatial period (Λ). It can be observed that with increasing period, the structure depth rises to a value of 0.92 μm at $\Lambda = 5$ μm. For $\Lambda =$ 10 μm, the depth was 0.75 μm ($F = 1.0$ J cm^{-2}). The minimal structure depth was found to be about 280 nm at $\Lambda =$ 500 nm (at 0.3 J cm^{-2}). In contrast, the aspect ratio increases with decreasing spatial period and shows a maximum of 0.55 for $\Lambda = 500$ nm and a minimum of 0.08 for $\Lambda = 10$ μm.

Orientation of Tumor Cells

PI substrates with periods of 500 nm, 1, 2, 5, and 10 μm were tested for their ability to guide mouse mammary adenocarcinoma cells (LM2). For comparison, the cells were also grown on nontreated PI samples. The spatial disposition of the LM2 tumor cells on nonpatterned and patterned PI surfaces and their morphology after incubation of 96 h is shown in Figure 4(a–f). The images correspond to the superposition of the optical microscopy picture and fluorescence microscopy with the nucleus of the cells stained with the DNA-specific fluorescent dye (Hoechst 33258). The arrows at the upper right corner of the images represent the orientation of the line-like structure.

As can be seen in Figure 4(a), the mostly multipolar cells show no specific direction but are rather randomly orientated and frequently overlapping on the nonpatterned surface. In

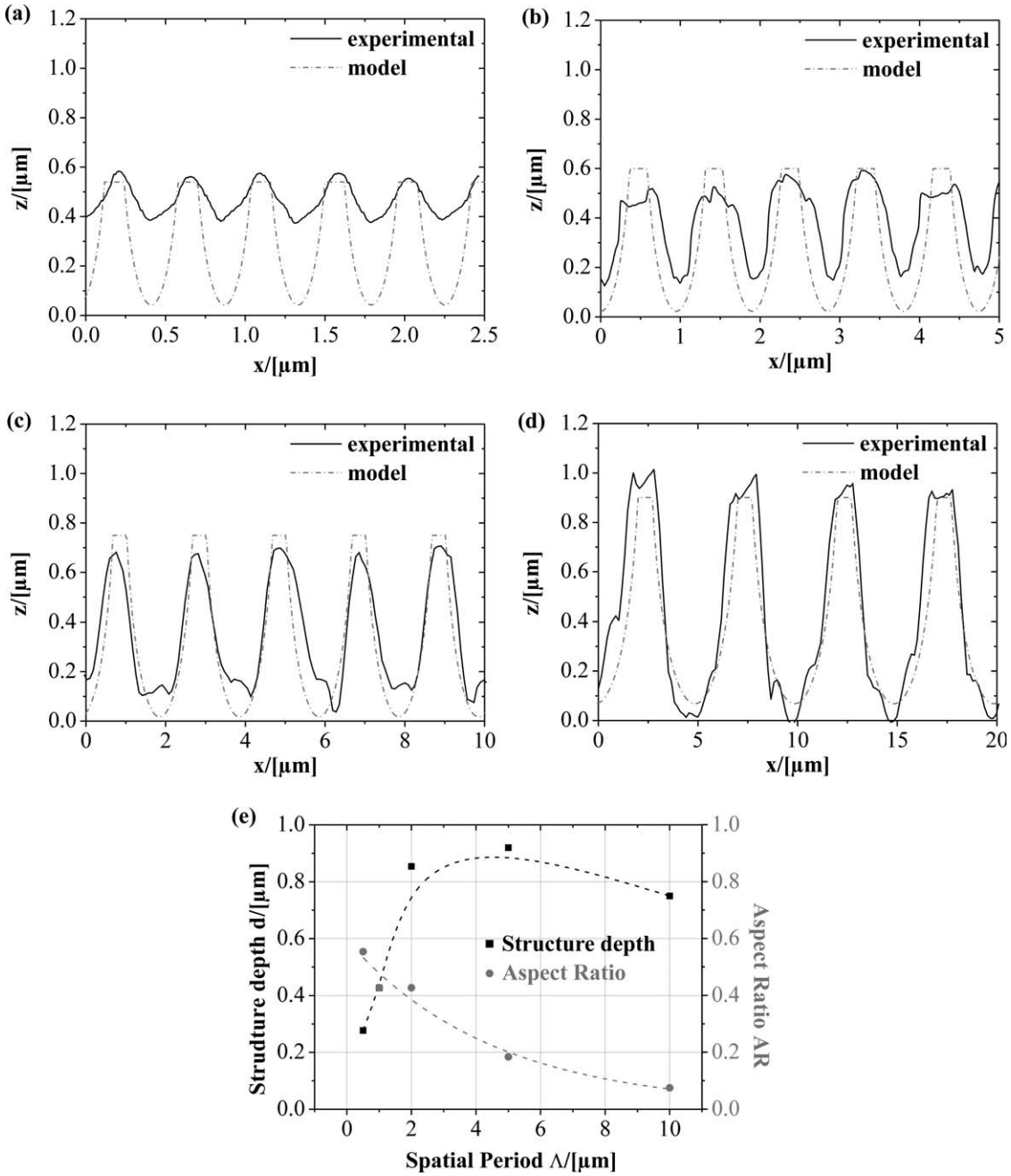

FIGURE 3 Experimental (dark) and simulated (light) surface profiles of the structured PI surface with spatial periods of (a) 500 nm ($F = 0.3$ J cm^{-2}), (b) 1 μm ($F = 0.5$ J cm^{-2}), (c) 2 μm ($F = 0.7$ J cm^{-2}), and (d) 5 μm ($F = 1.0$ J cm^{-2}). The experimental data were obtained from AFM (500 nm and 1 μm) and LSM (2 and 5 μm) measurements. (e) Structure depth and aspect ratio versus spatial period. The dotted lines are only for guiding the eyes.

contrast, the cells on the patterned surface are clearly orientated to the microstructure [Fig. 4(b–f)]. Particularly for smaller periods (500 nm to 2 μm), the cells are highly aligned to the direction of the structure [Fig. 4(b–d)], while also displaying a smaller size and an elongated morphology. On wider spatial periods of 5 and 10 μm [see Fig. 4(e,f)], it is possible to observe nonaligned cells.

The degree of alignment is shown in Figure 5. It can be seen that cells on the nonpatterned surface grow randomly without any preferential direction (with frequencies up to 20% for each 15° interval). In contrast, tumor cells attached to the patterned PI surfaces organize themselves in the direction of the line-like structure.

In Figure 6, the relative frequency of cell orientation between 0° and 15° is summarized for every spatial period, as well as the nonpatterned substrate. It is shown that while about 60% of the LM2 cells align at an angle of between 0° and 15° to the structure lines of periodicity

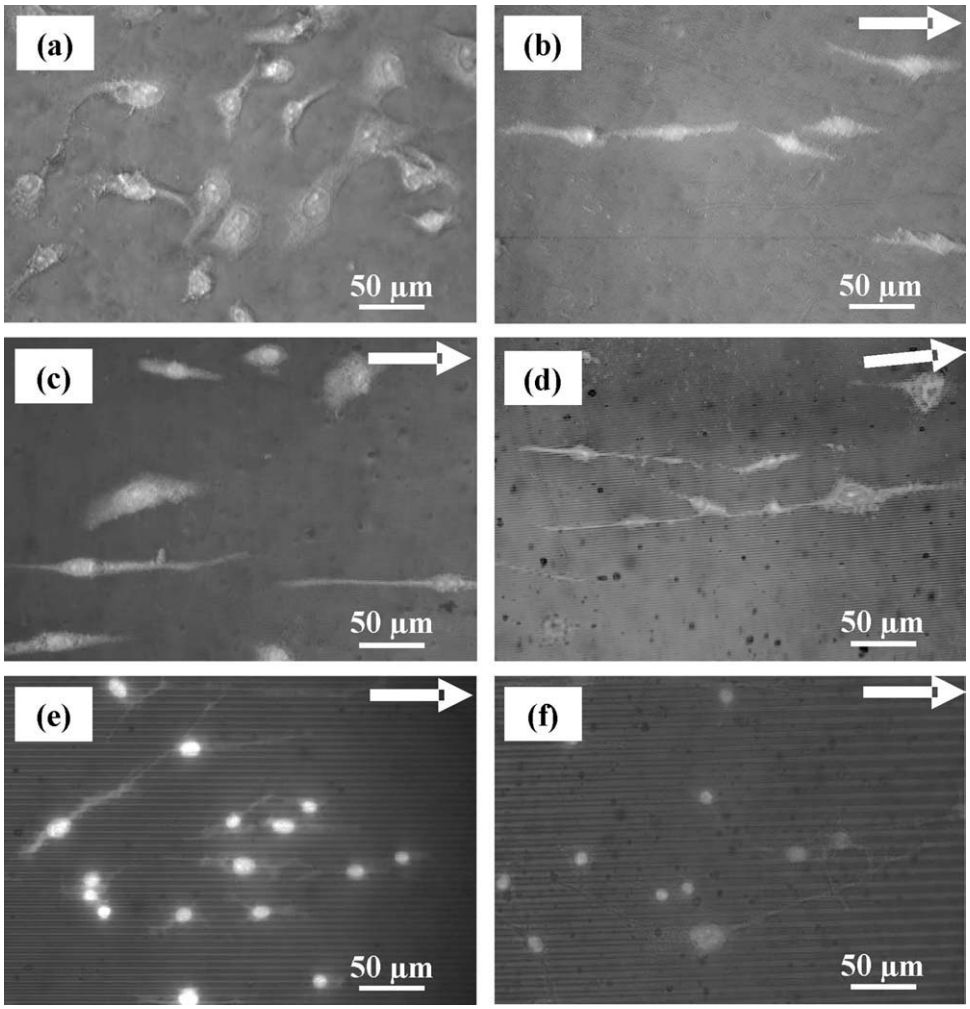

FIGURE 4 Fluorescence microscopy images of cells grown on (a) nonpatterned and patterned PI surfaces with spatial periods of (b) 500 nm, (c) 1 μm, (d) 2 μm, (e) 5 μm, and (f) 10 μm. The arrows indicate the direction of the line-like pattern.

5 and 10 μm, more than 70% are parallel to the lines with $\Lambda = 500$ nm to 2 μm.

DISCUSSION

The method of DLIP involves the formation of the spatial variation of intensity created by the interference of two or more laser beams.

For polymer materials showing high absorption coefficients for the adopted laser wavelength,[28–30] the intensity distribution of the interference pattern is transferred onto the material surface by photo-thermal, photo-chemical, or photo-physical processes. If electron excitation from the absorption of photons leads to chemical decomposition by direct bond breaking, then photo-chemical ablation is said to occur. Otherwise, the absorbed energy can produce vibrationally excited states, inducing melting and vaporization (photo-thermal ablation).[31,32]

For PI irradiated by light at wavelength 355 nm, both photo-chemical and photo-thermal ablation contributes to the removal of the material. This means that the PI is ablated by direct bond breaking and thermally induced vaporization processes.[31,33]

As the processes involved are highly complex, it is difficult to accurately correlate the reaction products with individual mechanisms.[34]

To calculate the shape of the ablated PI substrates using DLIP, a mathematical model was used, which combined the one-dimensional intensity distribution $I(x)$ for the two-beam interference case with a purely photo-chemical ablation model.

First, the shape of the periodic intensity distribution of the laser energy $I(x)$ is calculated using eq 2:

$$I(x) = I_0 \cos^2\left(x \frac{2\pi}{\lambda} \sin\alpha\right) \tag{2}$$

where I_0 is the summed laser intensity of the interfering laser beams.

The photochemical ablation $d(x)$ at position x is then calculated as function of the intensity $I(x)$ using eq 3:

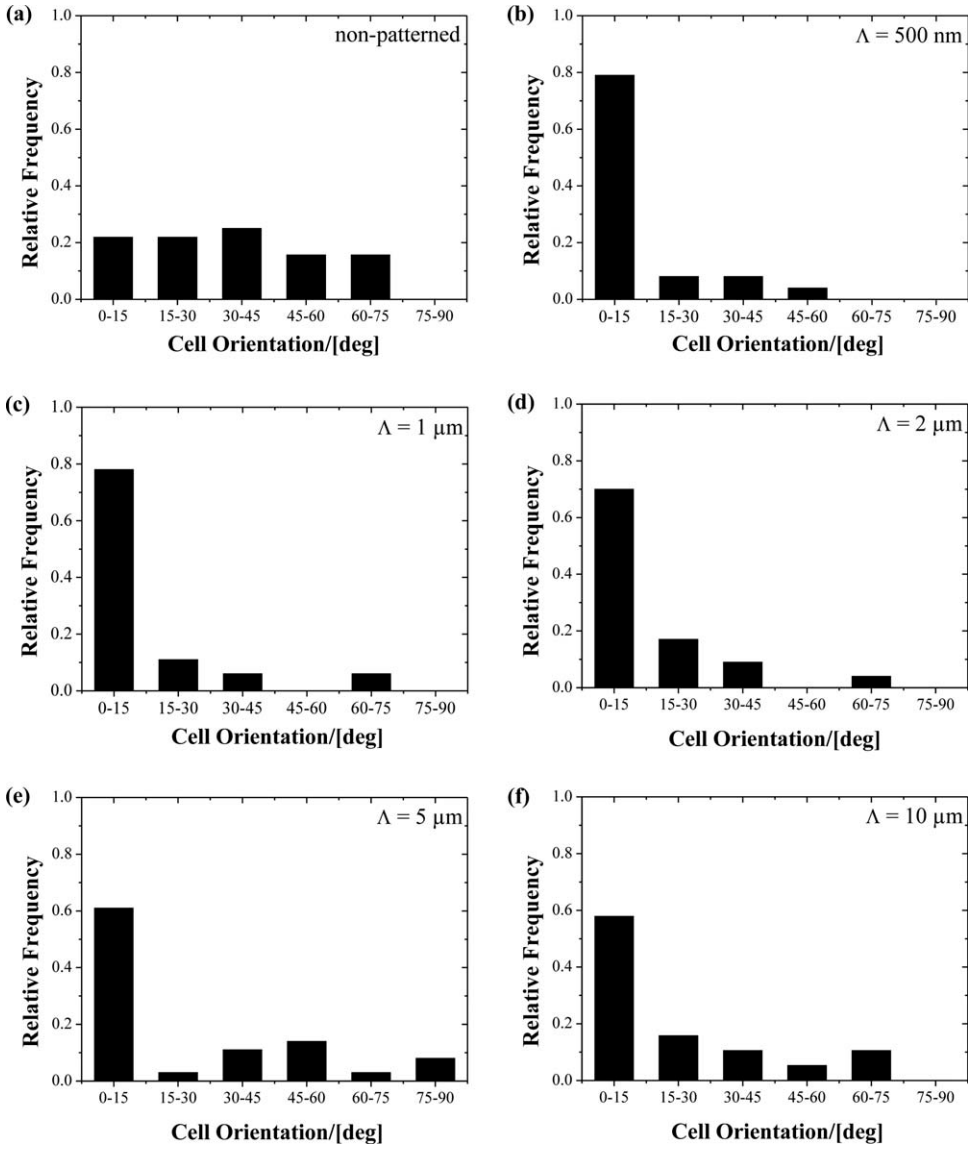

FIGURE 5 Orientation of LM2 cells after 96 h on nonpatterned and patterned PI surfaces (line-like structure, $\Lambda = 500$ nm to 10 μm).

$$d(x) = \begin{cases} \frac{1}{\kappa} \cdot \ln \frac{I(x)}{I_{th}} & I(x) \geq I_{th} \\ 0 & I(x) < I_{th} \end{cases} \quad (3)$$

where I_{th} denotes the threshold energy density necessary to induce material removal, and κ is the absorption coefficient. For PI, I_{th} and κ are 100 mJ cm^{-2} and $0.36 \cdot 10^5$ cm^{-1}.[30,35] Using eq 3, the surface profiles for the laser fluences depicted in Figure 3 (light lines) are calculated. The cross-sections derived from the mathematical model are in good agreement with the experimentally observed results for spatial periods of 5, 2, and 1 μm. It can be seen that the simulated ablation depth is very similar to the measured data for spatial periods larger than or equal to 1 μm. Concerning the topographical structure of the produced arrays, the patterns exhibit a well-defined shape [Fig. 2(b–d)], without the instabilities (defects) which predominate in other polymeric materials such polystyrene or polyethylene terephthalate, especially for periods below 1 μm. In these latter cases, the structuring process is controlled by photo-thermal ablation.[33,36]

The lower experimental structure depth d observed principally for 500 nm arrays can be explained as follows. Independent of the spatial period of the periodic array, the laser fluence and the nature of the polymer determine the amount of softened material on the polymer surface. In the case of a purely photo-chemical ablation process, the shape of the produced arrays should present well-defined sharp edges; the limiting physical property that determines the minimal reproducible spatial period is the thermal diffusion length (~1 to 10 nm for polymers irradiated with 10 ns pulses). In terms of photo-thermal effects, a softened or molten zone is produced (in addition to volatile products) which, in the case of DLIP, is evidenced by the peaks at the shoulders of the structure maxima [see e.g. Fig. 3(b,d)]. During the ablation process, the softened material at the interference

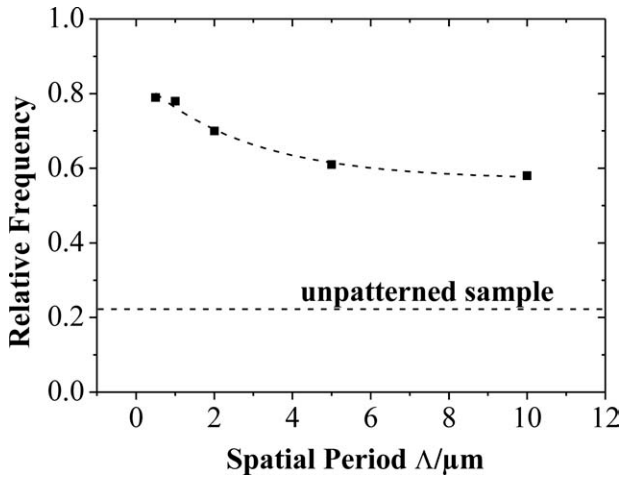

FIGURE 6 Relative frequency of orientation of the LM2 cells between 0° and 15° with respect to the lines (0°—parallel to lines). The dotted line is for eye guidance.

maxima is pulled out toward the minima positions due to the high pressure of the volatile ablation products. However, for small spatial periods (500 nm), the softened material cannot be completely removed from the maxima, and a lower ablation depth is observed compared with the calculated values. In consequence, the ablation depth seems to be limited by the photo-thermal effect (softened material) for short spatial periods.

Another important consideration during the ablation process is the modification of surface chemistry. During irradiation, a vapor and plasma plume containing electrons, ions, neutral fragments (e.g., carbon), and gaseous reaction products develops above the surface.[23,30] To some extent, the gaseous reaction products act like unstable free radicals, undergoing crosslinking reactions and forming carbon clusters.[35] These clusters, as well as the neutral fragments, redeposit on the samples as loosely attached debris (Fig. 2). Apart from such debris, which can be removed easily by ultrasonic bath, the surface chemistry does not change significantly after laser treatment as has been suggested by other authors.[35]

Cell growth experiments on the patterned PI substrates demonstrate that the mouse carcinoma mammary cells are mostly aligned to the pattern direction. The cells respond to the topography either by direct or indirect mechano-transduction.[37–41] This means that the surface of the micropattern provides mechanical stimuli, which cells are able to sense and respond to with a broad range of changes in shape, adhesion, migration, cell spreading, and differentiation.[42,43] One critical organelle thought to play an important role in the contact guidance response is the filopodium.[44] Filopodia are highly motile organelles involved in many cellular processes, including migration and sensing of local topography, which are able to detect the immediate environment.[45] For example, when in contact with ridges of the microstructure, the filopodia can detect these topographical features, causing the cell to exhibit a more elongated shape strongly orientated in the direction of the microstructure.[46]

In view of the average diameters of filopodia (200–400 nm),[47] it is likely that small spatial periods (500 nm to 1 μm) will influence cell growth.[2] This is confirmed by the presented results, which show that up to approximately 80% of the cells are orientated at an angle of less than 15° to lines with spatial periods of between 500 nm and 2 μm. This clearly indicates that mammary adenocarcinoma cells change their shape and behavior depending on substrate topography, as previously reported by authors using other cell types and substrates.[2,48–50]

CONCLUSIONS

Line-like structures with varying periods (500 nm to 10 μm) were fabricated on PI surfaces using the method of DLIP. Due to the predomination of photo-chemical ablation processes, the patterns exhibited good quality even at small periodic distances (500 nm), with structure depths between 0.3 (Λ = 500 nm) and 0.9 μm (Λ = 5 μm). These results were corroborated by mathematical calculations of such photochemical ablation processes. For small spatial periods, the calculated surface profiles overestimated the measured structure depth. One possible explanation for this phenomenon is the formation of softened material, which indicates that the photo-thermal aspect of the ablation process determines the structure depth for shorter spatial periods (500 nm).

Subsequently, the patterned samples were used for growth experiments of mouse mammalian adenocarcinoma cells. After incubating for 96 h, the cells showed an elongated morphology on the patterned PI and were strongly orientated in the direction of the line-like structure. The number of cells aligning to the pattern at an angle of less than 15° was seen to increase for shorter spatial periods (up to 80% of cells for 500 nm patterns). In summary, we conclude that DLIP is a suitable method for the rapid fabrication of periodic structures on large area polymeric substrates to control cell growth for biological and medical applications.

ACKNOWLEDGMENTS

This work was supported by FhG Internal Programs under Grant No. Attract 692 174. The International Bureau of the Federal Ministry of Education and Research, Germany, and the Ministry of Science and Technology, Argentina, are thanked for their financial support of this bilateral cooperative project in education and research (Project No. ARG 09/10).

REFERENCES AND NOTES

1 Angeli, F.; Brown, G.; Connolly, P.; Uttamchandani, D. *Micro Nano Lett.* **2006,** *1*, 66–70.

2 Anselme, K.; Davidson, P.; Popa, A. M.; Giazzon, M.; Liley, M.; Ploux, L. *Acta Biomater.* **2010,** *6*, 3824–3846.

3 Forbes, A.; Tomlins, P.; Gurdak, E.; Illsely, M.; James, S.; James, E. *J. Mater. Sci.: Mater. Med.* **2010,** *21*, 2463–2477.

4 Betancourt, T.; Brannon-Peppas, L. *Int. J. Nanomed.* **2006,** *I*, 483–495.

5 Wang, D.; Sun, G.; Chiou, B.-S. *Macromol. Mater. Eng.* **2008,** *293*, 657–665.

6 Ito, Y. *Biomaterials* **1999,** *20*, 2333–2342.

7 Zhu, B.; Zhang, Q.; Lu, Q.; Xu, Y.; Yin, J.; Hu, J.; Wang, Z. *Biomaterials* **2003,** *25*, 4215–4223.

8 Gomez, N.; Lee, J. Y.; Nickels, J. D.; Schmidt, C. E. *Adv. Funct. Mater.* **2007,** *17*, 1645–1653.

9 Cui, X.; Lee, V. A.; Raphael, Y.; Wiler, J. A.; Hetke, J. F.; Anderson, D. J.; Martin, D. C. *J. Biomed. Mater. Res.* **2001,** *56*, 261–272.

10 Collier, J. H.; Camp, J. P.; Hudson, T. W.; Schmidt, C. E. *J. Biomed. Mater. Res.* **2000,** *50*, 574–584.

11 Stauffer, W. R.; Cui, X. T. *Biomaterials* **2006,** *27*, 2405–2413.

12 Cui, X.; Wiler, J.; Dzaman, M.; Altschuler, R. A.; Martin, D. C. *Biomaterials* **2003,** *24*, 777–787.

13 Cen, L.; Neoh, K. G.; Li, Y.; Kang, E. T. *Biomacromolecules* **2004,** *5*, 2338–2346.

14 Sanghvi, A.; Miller, K. P.; Belcher, A. M.; Schmidt, C. E. *Nat. Mater.* **2005,** *4*, 496–502.

15 Yang, J.; Martin, D.C. *Sens. Actuators B* **2004,** *101*, 133–142.

16 Jiang, L.; Wang, X.; Xi, L. *Small* **2011,** *7*, 1309–1321.

17 Gallagher, J. O.; McGhee, K. F.; Wilkinson, C. D.; Riehle, M. O. *IEEE Trans. Nanobiosci.* **2002,** *1*, 24–28.

18 Wan, Y.; Wang, Y.; Liu, Z.; Qu, X.; Han, B.; Bei, J.; Wang, S. *Biomaterials* **2005,** *26*, 4453–4459.

19 Lim, J. Y.; Hansen, J. C.; Siedlecki, C. A.; Runt, J.; Donahue, H. J. *J. R. Soc. Interface* **2005,** *2*, 97–108.

20 Dalby, M. J.; Giannaras, D.; Riehle, M. O.; Gadegaard, N.; Affrossman, S.; Curtis, A. S. *Biomaterials* **2004,** *25*, 77–83.

21 Ni, M; Hao Tong, W.; Choudhury, D.; Rahim, N. A. A.; Iliescu, C.; Yu, H. *Int. J. Mol. Sci.* **2009,** *10*, 5411–5441.

22 Geppert, L. *IEEE Spectrum* **1996,** *33*, 33–38.

23 Bäuerle, D. Laser Processing and Chemistry, 2nd ed.; Springer (Berlin, Heidelberg), **1996; Chapter 12, pp 191.**

24 Dumont, Th.; Bischofberger, R.; Lippert, T.; Wokaun, A. *Appl. Surf. Sci.* **2005,** *247*, 115–122.

25 Lasagni, A.; Acevedo, D.; Barbero, C.; Mücklich, F. *Adv. Eng. Mater.* **2007,** *9*, 99–103.

26 Acevedo, D.; Lasagni, A.; Barbero, C.; Mücklich, F. *Adv. Mater.* **2007,** *19*, 1272–1275.

27 Yu, F.; Mücklich, F.; Li, P; Shen, H.; Mathur, S.; Lehr, C.-M.; Bakowsky, U. *Biomacromolecules* **2005,** *6*, 1160–1167.

28 Dyer, P. E. *Appl. Phys. A* **2003,** *77*, 167–173.

29 Koren, G.; Yeh, Y. T. C. *J. Appl. Phys.* **1984,** *56*, 2120–2126.

30 Küper, S.; Brannon, J.; Brannon, K. *Appl. Phys. A* **1993,** *56*, 43–50.

31 Yung, W. K. C.; Liu, J. S.; Man, H. C.; Yue, T. M. *J. Mater. Proc. Technol.* **2000,** *101*, 306–311.

32 Srinivasan, R.; Braren, B. *Chem. Rev.* **1989,** *I9SS. 89*, 1303–1316.

33 Lasagni, A.; Roch, T.; Bieda, M.; Langheinrich, D. *Laser Technik J.* **2011,** *8*, 45–48.

34 Lippert, T. In Laser-Surface Interactions for New Materials Production Tailoring Structure and Properties, Springer Series in Material Chemistry, Vol. *130*, Eds. Miotello, A. Ossi, P. M. Springer Verlag: Berlin, **2009; pp 141.**

35 Yung, K. C.; Zeng, D. W.; Yue, T. M. *Appl. Surf. Sci.* **2001,** *173*, 193–202.

36 Frey, M. T.; Tsai, I. Y.; Russell, T. P.; Hanks, S. K.; Wang, Y. L. *Biophys. J.* **2006,** *90*, 3774–3782.

37 Wang, J. H.; Thampatty, B. P.; Lin, J. S.; Im, H. J. *Gene* **2007,** *391*, 1–15.

38 Forgcas, G. *J. Cell. Sci.* **1995,** *108*, 2131–2143.

39 Ingber, D. E. In Cell Mechanics and Cellular Engineering; Van, V.; Mow, F.; Guilak, R.; Tran-Son-Tay, R. M.; Hochmuth, R. M., Eds.; Springer: New York, **1994; pp 329.**

40 Ingber, D. E. *J. Cell. Sci.* **1993,** *104*, 613–627.

41 Ingber, D. E. *Curr. Opin. Cell. Biol.* **1991,** *3*, 841–848.

42 Lim, Y.; Dreiss, A. D.; Zhou, Z.; Hansen, J. C.; Siedlecki, C. A.; Hengstebeck, R. W. *Biomaterials* **2007,** *28*, 1787–1797.

43 Dalby, M. J.; Pasqui, D.; Affrossman, S. *IEEE Proc. Nanobiotechnol.* **2004,** *151*, 53–61.

44 Dalby, M. J.; Gadegaard, N.; Riehle, M. O.; Wilkinson, C.; Curtis, A. *Int. J. Biochem. Cell B* **2004,** *36*, 2005–2015.

45 Bettinger, C. J.; Langer, R.; Borenstein, J. T. *Angew. Chem. Int. Ed. Engl.* **2009,** *48*, 5406–5415.

46 Fujita, S.; Ohshima, M.; Iwata, H. *J. R. Soc. Interface* **2009,** *6*, S269–S277.

47 MacClay, D. R. *Exp. Cell Res.* **1999,** *253*, 296–301.

48 Curtis, A.; Wilkinson, C. *Biomaterials* **1997,** *18*, 1573–1583.

49 Walboomers, X. F.; Monaghan, W.; Curtis, A.; Jansen, J. A. *J. Biomed. Res.* **1999,** *46*, 212–220.

50 Teixeira, A. I.; Abrams, G. A.; Bertics, P. J.; Murphy, C. J.; Nealey, P. F. *J. Cell. Sci.* **2003,** *116*, 1881–1892.